Journal of Power Sources 244 (2013) 164–169

Contents lists available at SciVerse ScienceDirect

Journal of Power Sources

journal homepage: www.elsevier.com/locate/jpowsour

Facile synthesis of hierarchical mesoporous $Li_4Ti_5O_{12}$ microspheres in supercritical methanol

Agung Nugroho [a,c], Su Jin Kim [b], Wonyoung Chang [b], Kyung Yoon Chung [b], Jaehoon Kim [d,e,*]

[a] Supercritical Fluid Research Laboratory, Clean Energy Research Center, Korea Institute of Science and Technology, Hwarangno 14-gil 5, Seongbuk-gu, Seoul 136-791, Republic of Korea
[b] Center for Energy Convergence, Korea Institute of Science and Technology, Republic of Korea
[c] Clean Energy and Chemical Engineering, University of Science and Technology, 113 Gwahangno, Yuseong-gu 305333, Daejeon, Republic of Korea
[d] School of Mechanical Engineering, Sungkyunkwan University, 2066, Seobu-Ro, Jangan-Gu, Suwon, Gyeong Gi-Do 440-746, Republic of Korea
[e] SKKU Advanced Institute of Nano Technology (SAINT), 2066, Seobu-Ro, Jangan-Gu, Suwon, Gyeong Gi-Do 440-746, Republic of Korea

HIGHLIGHTS

- Hierarchical mesoporous $Li_4Ti_5O_{12}$ microsphere synthesized in supercritical methanol.
- Fast synthesis with no template or surfactant used.
- $Li_4Ti_5O_{12}$ shows excellent long-term cyclability and high-rate capability.
- Much better performance than that from supercritical water and solid-state methods.

ARTICLE INFO

Article history:
Received 2 October 2012
Received in revised form
27 January 2013
Accepted 22 February 2013
Available online 4 March 2013

Keywords:
Lithium titanate
Supercritical methanol
Mesoporous
Lithium-ion batteries

ABSTRACT

A facile, template-free route using supercritical methanol for the preparation of hierarchical mesoporous $Li_4Ti_5O_{12}$ spinel microspheres in a very short reaction time is introduced. Nanosized, primary $Li_4Ti_5O_{12}$ particles (5–10 nm) are loosely aggregated and form micron-sized, secondary mesoporous spheres (0.2–2.0 μm) with a pore size of 2–10 nm. Subsequent calcination of the as-synthesized $Li_4Ti_5O_{12}$ at a low temperature of 600 °C results in excellent long-term cyclability and high rate performance. The discharge capacity after 400 cycles at 1 C is 134.9 mAh g^{-1} (77.6% of the initial discharge capacity), and the discharge capacity at 10 C is 108.5 mAh g^{-1}. The formation mechanism of hierarchical mesoporous microspheres in supercritical methanol is discussed.

1. Introduction

Because of the current issues of global warming and fossil fuel depletion, extensive efforts have been made to develop renewable and sustainable energy sources and energy storage materials. Large-scale Li-ion batteries have received considerable attention not only as power sources for plug-in hybrid electric vehicles (PHEV) and electric vehicles (EV), but also for energy storage applications [1,2]. For such applications, Li-ion batteries with high power density, high energy density, high safety, long cycle life, and low production cost are essential. Spinel lithium titanium oxide ($Li_4Ti_5O_{12}$, LTO) has been considered to be a promising anode material for large-scale Li-ion battery applications. This is because LTO possesses excellent reversibility and durability due to almost no structural change during Li ion insertion/extraction, it is safe due to its high flat discharge voltage at around 1.55 V (vs. Li/Li^+), and the cost of Ti is low [3–5].

In spite of these advantages, the power density of LTO at high charge/discharge rates is relatively poor because of its extremely low electronic conductivity ($\sim 10^{-13}$ S cm^{-1}) [6] and sluggish lithium ion diffusivity ($\sim 10^{-12}$ cm^2 s^{-1}) [7], which often fail to satisfy the requirements of large-scale applications. To date, many approaches have been developed for enhancing the rate capability of LTO. One approach is to employ doping with foreign atoms and electronically conductive coatings on LTO [8–13]. Another

* Corresponding author. School of Mechanical Engineering, Sungkyunkwan University, 2066, Seobu-Ro, Jangan-Gu, Suwon, Gyeong Gi-Do 440-746, Republic of Korea. Tel.: +82 31 299 4843; fax: +82 31 290 5889.
E-mail addresses: jaehoonkim@skku.edu, kjh0508@gmail.com (J. Kim).

0378-7753/$ – see front matter
http://dx.doi.org/10.1016/j.jpowsour.2013.02.070

approach is to employ nanostructured morphologies because the reduced particle size can facilitate Li ion and electron transport kinetics by reducing the path lengths and by increasing the electrode-electrolyte interphase area [14–16]. Previous research has demonstrated that the rate capability can be significantly improved by employing nanostructured LTO, e.g., nanoparticles [15], nanotubes [17], nanorods [18], nanowires [19], nanosheets [20] and nanoflowers [21]. However, the use of nanomaterials for the fabrication of electrodes causes low volumetric energy density and inhomogeneous active material coating, both of which present challenges for practical applications [22,23].

One of potential strategies for overcoming the problems associated with nanostructured LTO is the design of hierarchical porous structures in which nanosized primary particles aggregate and form micron-sized secondary porous materials [5,22,24–35]. The porous morphology exhibits the advantages of both nanostructure morphology (e.g., fast Li ion intercalation/deintercalation, fast electron diffusion, large electrode-electrolyte interphase area, etc.) and micron-sized assembly (e.g., high volumetric density, easy processability, stability, etc.). In addition, the electrolytes can penetrate the porous structure resulting in good contact with the primary particles and high utilization of the active material. Hierarchical porous LTO has been fabricated using various types of templates such as monodisperse polymer colloidal crystals [5,32], block copolymers [25,28], and carbon spheres [27]. The use of templates and the requirement of template removal often make the synthetic process complicated and costly. A simple, template-free method that is capable of controlling the primary particle size and mesoporosity would be a more advantageous approach. Various template-free methods have been developed, including hydrothermal methods [22,24,29–31], solvothermal methods [33,36], and a method that combines ball milling with spray drying [26,34,35]. The hierarchical LTO synthesized using these methods exhibited high rate capabilities, excellent cycling performances, and high energy density. However, most of the previous template-free methods were time-consuming (12–24 h) or required multi-step processes to obtain the final products. Therefore, the development of simpler, more reliable, and faster methods to prepare hierarchical LTO with rich mesoporosity still remains a great challenge.

This work describes the first use of supercritical methanol (scMeOH) to synthesize hierarchical LTO microspheres assembled with uniform, nanosized LTO particles. The key features of this scMeOH approach are that it is a very simple, template-free, and fast method to obtain mesoporous LTO materials. We demonstrate that hierarchical LTO microspheres can be prepared in scMeOH in a very short reaction time (less than 15 min) without utilizing structure-directing chemicals. LTO subsequently calcinated at a mild temperature (600 °C) exhibits excellent rate performance and long-term cyclability when tested as an anode in lithium ion batteries.

2. Experimental

In a typical synthesis, 14.27 mg $LiOH \cdot H_2O$ (purity 98 wt%, Sigma–Aldrich, USA) and 122.1 mg titanium tetraisopropoxide (TTIP, purity 97 wt%, Sigma–Aldrich, USA) were charged into 3.5 mL methanol and the suspension was transferred into a SUS316 tube reactor with an inner volume of 11 mL. The reactor was then heated in a molten salt bath whose temperature was maintained at 400 °C. The pressure of the reactor was increased to 30 MPa in 1 min. After 15 min, the resulting precipitates were washed with methanol carefully to remove residual organic constituents followed by vacuum drying at 80 °C for 12 h. Finally, 16.6 mg of a yellowish white powder was obtained. The sample, referred to as LTO-scMeOH, was calcinated at temperatures of 500, 600, and 700 °C for 12 h in an air flow. The samples calcinated at 500, 600, and 700 °C were referred to as LTO-scMeOH-500C, LTO-scMeOH-600C, and LTO-scMeOH-700C, respectively.

The crystal structures of the samples were characterized by X-ray diffraction (XRD, Rigaku RINT2000, Tokyo, Japan) with Cu Kα radiation at 40 kV and 50 mA. The functional groups on the surface of LTO were characterized using a NICOLET 380 FT-IR spectrometer (Thermo Electron Co. NJ, USA). The thermal properties of the obtained particles were measured using a DuPont Instruments TGA 2950 thermal analyzer. The particle morphologies were observed

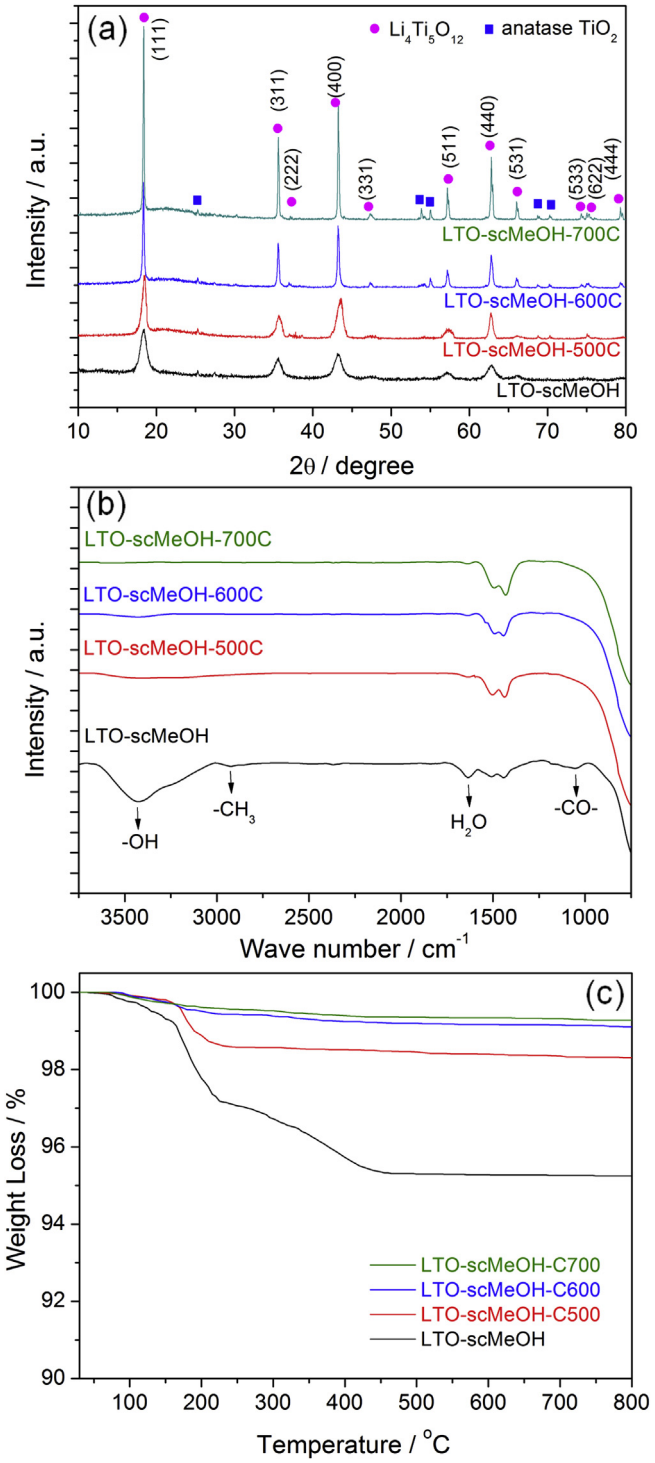

Fig. 1. (a) XRD patterns, (b) FT-IR spectra, and (c) TGA graphs of LTO-scMeOH, LTO-scMeOH-500C, LTO-scMeOH-600C, and LTO-scMeOH-700C.

using a field emission scanning electron microscope (FE-SEM, Hitachi S-4100, Tokyo, Japan) and high-resolution transmission electron microscope (HR-TEM, Tecnai FT20, FEI Co., OR, USA). The Brunauer–Emmett–Teller (BET) surface area and the microstructural properties were determined using a BELSORP-mini II apparatus (BEL Japan Inc., Osaka, Japan). The charge–discharge properties of the prepared LTO anode materials were measured in 2032 coin-type cells using metallic lithium foil as the counter electrode. The active material (87 wt%), acetylene black as a conducting material (7 wt%), and polyvinylidene fluoride (PVDF) as a binder (6 wt%) in NMP were mixed using a homogenizer (Nihonseiki Kaisha LTD. Tokyo, Japan). The slurry was then coated onto Cu foil. After vacuum drying at 80 °C for 24 h, electrode discs with a diameters of 15 mm (area of 1.77 cm^2) were punched out and weighed. The electrolyte was 1 M $LiPF_6$ dissolved in ethylene carbonate/dimethyl carbonate/ethylmethyl carbonate solvent (volume ratio of EC:DMC:EMC = 1:1:1). A microporous polypropylene membrane with a pore size of 25 μm (Celgard 2500, Celgard LLC., Charlotte, NC) was used as the separator. The cell assembly was conducted in a dry room. The cells were galvanostatically charged and discharged in a voltage range of 1.0–2.5 V (vs. Li/Li^+) using a Maccor Series 4000 Battery Test System (Oklahoma, USA) at room temperature. The long-term cyclability was recorded at a rate of 1 C (1 C = 175 mA g^{-1}) for up to 400 cycles. The charge–discharge rate was varied from 1 C to 20 C for rate performance measurements.

3. Results and discussion

Fig. 1a shows the XRD patterns of the LTO samples prepared in scMeOH and subsequently calcinated at different temperatures. All main diffraction peaks observed for LTO synthesized in scMeOH with a reaction time of 15 min (LTO-scMeOH) were assigned to the spinel LTO pattern (JCPDS No.49-0207). The most intense peaks at 18.4°, 35.6°, 43.3°, and 62.8° respectively correspond to the (111), (311), (400), and (440) reflections of the LTO spinel structure. A trace amount of the impurity phase can be also seen at 18.4°, which corresponds to the (101) reflection of anatase TiO_2 (see Fig. S1a, Supplementary data). The crystallite size estimated using the Scherrer equation and (111) peak was estimated to be 4.9 nm, confirming the formation of nanocrystalline LTO. This suggests that LTO can be facilely synthesized in scMeOH in the very short reaction time of 15 min.

When the sample was calcinated at 500 °C (LTO-scMeOH-500C), the XRD pattern did not change significantly. At higher calcination temperatures of 600 and 700 °C (LTO-scMeOH-600C and LTO-scMeOH-700C, respectively), the main peaks associated with the LTO phase became sharper and narrower, indicating an increase in crystallinity. The crystallite size was estimated to be 11.1, 23.7, and 62.1 nm after the calcinations at 500, 600, and 700 °C, respectively. The anatase TiO_2 peak at 18.4° that was present in LTO-scMeOH persisted after calcination (Fig. S1a). As shown in Fig. S1b, other anatase TiO_2 peaks at 53.9° and 55.0° were observed at the calcination temperatures of 600 and 700 °C. However, such trace amounts of the impurity phases have a negligible effect on the electrochemical performance, as will be discussed later. The surface functional groups were examined by FT-IR spectroscopy, and the results are shown in Fig. 1b. The FT-IR spectrum of the LTO-scMeOH exhibits a (–CO–) stretching peak at 1050 cm^{-1}, methyl (-CH_3) stretching peak at 2926 cm^{-1}, and –OH stretching peak at 3000–3750 cm^{-1}, suggesting that scMeOH acts as a methylation, hydroxylation, and methoxylation agent [37,38]. Similar surface modifications have been observed in CeO_2 and ZnO nanoparticles synthesized in scMeOH [37–40]. The peak at 1637 cm^{-1} is due to adsorbed water on the surface of the LTO sample [41]. After calcination in air, the surface functional groups disappeared due to organic species burn-off. Fig. 1c shows the thermal properties of the LTO samples determined by thermal gravimetric analysis (TGA). The weight loss of LTO-scMeOH over the course of increasing temperature up to 800 °C was ~4.7%. The weight loss curve at 250–450 °C can be attributed to the detachment of functional groups that were present on the surfaces of the nanoparticles. This indicates that the surfaces of the uncalcinated particles were

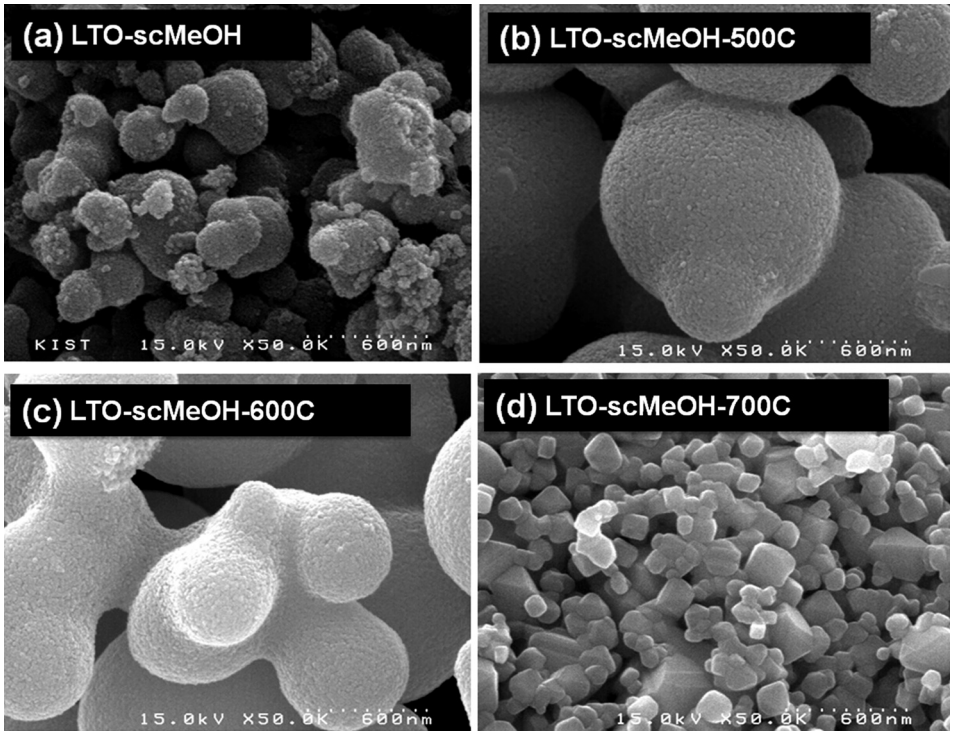

Fig. 2. SEM images of (a) LTO-scMeOH, (b) LTO-scMeOH-500C, (c) LTO-scMeOH-600C, and (d) LTO-scMeOH-700C.

covered by organic species, which agrees well with the FT-IR results. The weight loss of LTO-scMeOH-500C decreased to 1.7% and that of the samples calcinated at 600 and 700 °C became negligible. This suggests that the organic species present at the surface of LTO were removed after calcination at 600 and 700 °C.

The morphology of the synthesized samples was examined by FE-SEM and the images are shown in Fig. 2. LTO-scMeOH particles are spherical with diameters of 0.2–2.0 μm. The high resolution image in Fig. S2 shows that the microspheres are comprised of many of ultrafine nanoparticles. Irregular-shape pore structure is clearly seen between the interconnected nanoparticles. The unique mesoporous nano/micro morphology of the particles synthesized in scMeOH may be due to the presence of organic species attached to the particles. At the initial stage of nucleation, the surface of the particle is covered by the organic species, prohibiting further growth, for example, by the Ostwald ripening mechanism. The surface-modified nanoparticles were slightly agglomerated and formed micron-sized spherical particles, e.g., by interparticle interactions, leaving empty space among the nanoparticles. The hierarchically mesoporous microsphere morphology was maintained at the calcination temperatures of 500 and 600 °C, as shown in Fig. 2b–c and Fig. S3. At the high calcination temperature of 700 °C, however, significant interparticle aggregation between neighboring particles led to the collapse of the mesoporous morphology.

The architectural and textural properties of the synthesized particles were further examined by TEM, HR-TEM and BET

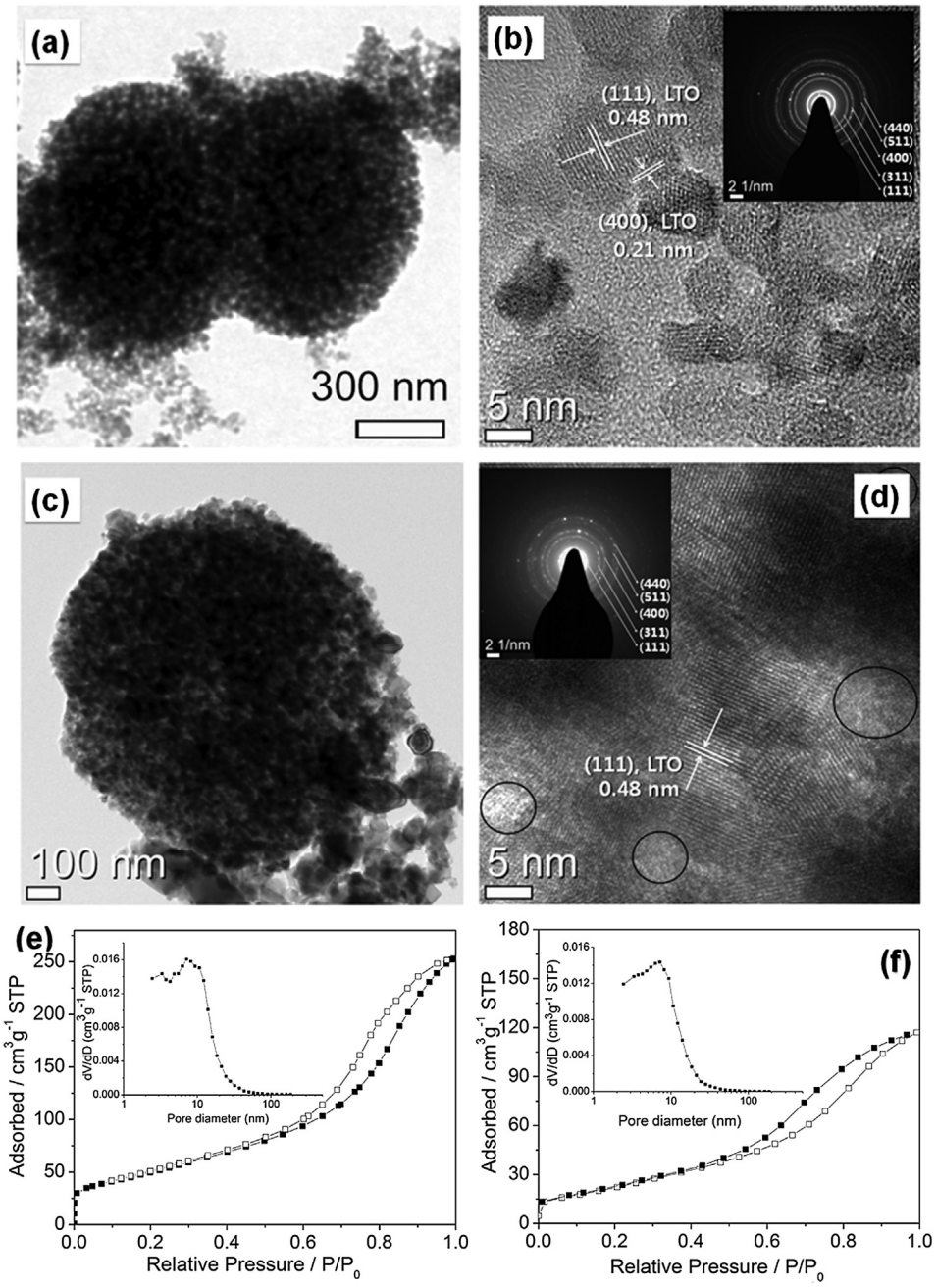

Fig. 3. (a) TEM, (b) HR-TEM, and (e) BET results for LTO-scMeOH and (c) TEM, (d) HR-TEM, and (f) BET results for LTO-scMeOH-600C. The circles in (d) indicate pores between the particles.

measurements. The TEM and HR-TEM images of LTO-scMeOH (Fig. 3a and b) confirm that the microsphere consists of interconnected nanocrystallites with sizes in the range of 5–10 nm. The size of the nanocrystallites was in good agreement with that estimated from XRD. The lengths of atomic rows in the nanocrystallites were 0.48 and 0.21 nm and correspond to the (111) and (400) planes of the LTO phase, respectively. The lattice fringes in the selected area electron diffraction (SAED) shown in the inset of Fig. 3b also confirm that the nanocrystallite retained the LTO phase and indicates that the nanocrystallites are randomly oriented with respect to each other. Many pores with sizes of 2–10 nm around the primary nanocrystallites are clearly visible in Fig. 3b, confirming the presence of porous structure. As shown in Fig. 3c and d, calcination at 600 °C led to an increase in the primary particle size to 30–100 nm without changing the hierarchical mesoporous morphology. The increase in the crystallite size led to a decrease in BET surface area from 117.4 $m^2 g^{-1}$ to 57.8 $m^2 g^{-1}$ after calcinations. The porous structure was further examined by nitrogen absorption–desorption isotherms. As shown in Fig. 3e, the isotherm of LTO-scMeOH exhibits a distinct hysteresis at P/P_o of 0.6–1.0, indicating the presence of mesoporous structure. The corresponding Barrett–Joyner–Halenda (BJH) pore size distribution curve (inset) shows that the pore size of LTO-scMeOH is not uniform and ranges between 2 and 10 nm with an average pore size of 8.3 nm. After calcination at 600 °C, the hysteresis loop was still observed at P/P_o of 0.6–1.0. The average pore size (8.4 nm) and pore size distribution of LTO-scMeOH-600C are very similar to those of LTO-scMeOH. This clearly indicates that the hierarchically mesoporous microsphere morphology was retained after calcination at 600 °C, which agrees well with the SEM and TEM results.

Fig. 4 shows the electrochemical performance of LTO-scMeOH and LTO-scMeOH-600C in the potential range of 1.0–2.5 V versus Li/Li^+. For comparison purposes, the electrochemical properties of micrometer-sized LTO particles that were synthesized by a solid-state method (LTO-SS) and submicrometer-sized LTO particles that were synthesized in supercritical water and subsequently calcinated at 700 °C (LTO-scH_2O-700C) are also shown in the figure. The BET surface area of LTO-SS and LTO-scH_2O-700C were 5.4 and 10.0 $m^2 g^{-1}$, respectively. Details on the preparation procedures and characteristics of LTO-SS and LTO-scH_2O-700C are described in our previous papers [42,43]. The charge-discharge voltage profile of LTO-scMeOH exhibits sloping voltage plateaus and an initial discharge capacity of 48.5 mAh g^{-1}, which is considerably lower than the theoretical value (175 mAh g^{-1}). This suggests that not all of the active materials were properly utilized. The poor electrochemical performance of LTO-scMeOH is probably due to the unstable spinel structure and poor crystallinity. After the sample was calcinated at 600 °C, significantly enhanced electrochemical performance was observed. The charge-discharge curve of LTO-scMeOH-600C shows an extremely flat voltage profile at approximately 1.55 V. The initial discharge capacity (173.9 mAh g^{-1}) almost reached the theoretical value, suggesting that the increase in crystallinity contributed to the higher discharge capacity. The initial discharge capacities of the submicrometer-sized LTO-scH_2O-700C (149.6 mAh g^{-1}) and the micrometer-sized LTO-SS (105.2 mAh g^{-1}) are much lower than that of LTO-scMeOH-600C.

The hierarchical mesoporous LTO microspheres synthesized using scMeOH show excellent rate performance. The samples were progressively charged and discharged at 17.5 mA g^{-1} (0.1 C), 175 mA g^{-1} (1 C), 350 mA g^{-1} (2 C), 700 mA g^{-1} (4 C), 1400 mA g^{-1} (8 C), 1750 mA g^{-1} (10 C), and 3500 mA g^{-1} (20 C), as shown in Fig. 4b. LTO-scMeOH-600C exhibits much higher specific discharge capacities at current rates up to 20 C than those of LTO-SS. The capacity of LTO-scMeOH-600C was 155.6 mAh g^{-1} at 4 C and 79.7 mAh g^{-1} at 20 C whiles the capacities of micron-sized LTO-SS were 96.5 mAh g^{-1} at 4 C and 25.8 mAh g^{-1} at 20 C. When compared to the submicrometer-sized LTO-scH_2O-700C, the mesoporous LTO showed much better performance up to 8 C, while its rate performance became comparable to that of LTO-scH_2O-700C at higher current rates. The better rate performance of LTO-scMeOH-700C could be due to the mesoporous channel which allows the electrolytes to penetrate the structure, resulting in much higher interfacial contact with nanosized LTO building blocks and better

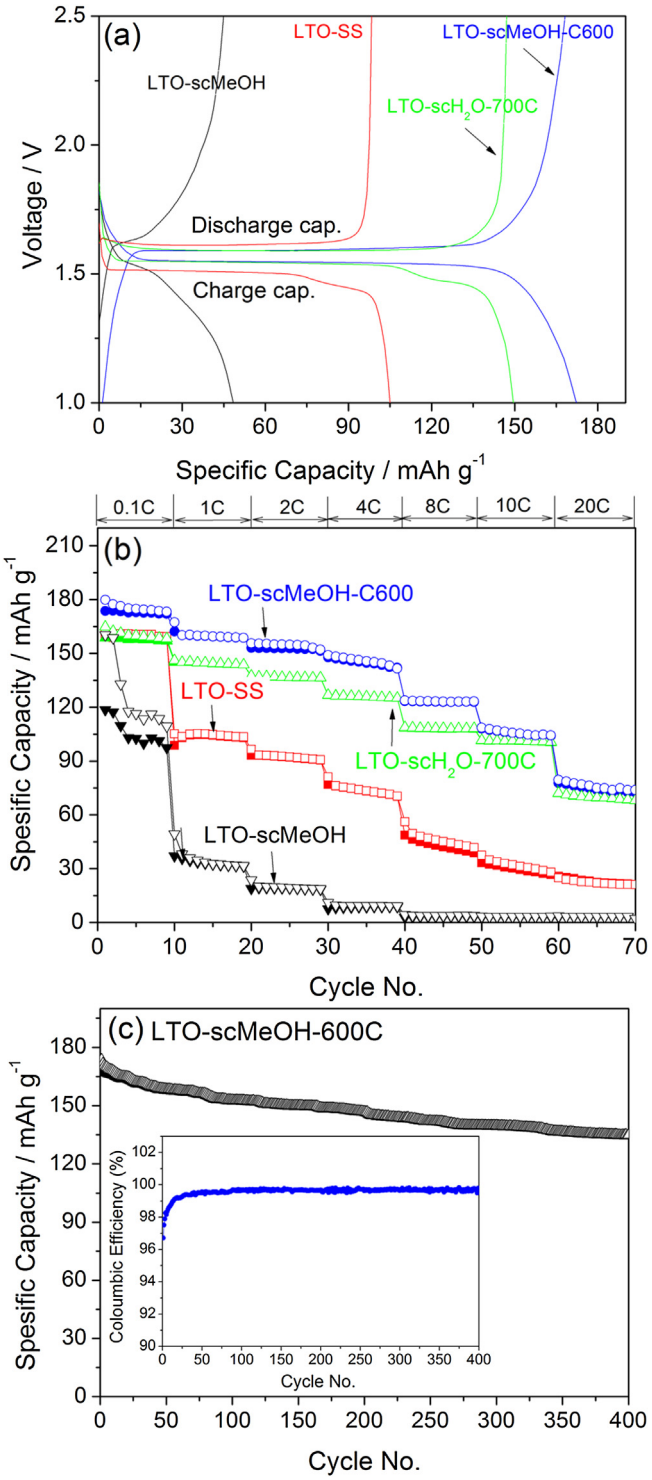

Fig. 4. Electrochemical properties of LTO-scMeOH, LTO-scMeOH-600C, LTO-SS, and LTO-scH_2O-700C.

accessibility of the active material. Lastly, the mesoporous LTO microspheres exhibit excellent capacity retention. Fig. 4c shows the cycling performance of LTO-scMeOH-600C for up to 400 cycles at 1 C. The discharge capacity after 400 cycles was 134.9 mAh g^{-1}, which is 77.6% of the initial discharge capacity (173.7 mAh g^{-1}). The coulombic efficiency, shown in the inset of Fig. 4c, was almost 100% after 15 cycles. The outstanding cycling performance can be attributed to good structural integrity and high crystallinity of the LTO microspheres. However, the specific capacity of the hierarchical mesoporous LTO microspheres proposed here is still lower than that the required for practical use. Takami and coworkers proposed to synthesize Nb containing LTO ($TiNb_2O_7$) whose specific capacity is as high as 300 mAh g^{-1} [44]. For the purpose of practical application of our proposed method, we will try to synthesize $TiNb_2O_7$ in the supercritical fluids in the near future.

4. Conclusions

In summary, we have developed a simple, fast, and template-free method for fabricating hierarchical mesoporous LTO microspheres. This method is based on a scMeOH process followed by calcination at low temperatures. The mesoporous LTO microspheres synthesized using this method exhibit high rate performance, high capacity, and long-term cyclability, which clearly indicate that this is a very promising approach for the efficient utilization of active material in large-scale lithium battery applications.

Acknowledgments

This research was supported by the KIST Young Fellow Program of the Korea Institute of Science and Technology. The authors also acknowledge support from the Global Research Lab (GRL) Program through the National Research Foundation of Korea (NRF) funded by the Ministry of Education, Science and Technology (MEST) (grant number: 2011-00115).

Appendix A. Supplementary data

Supplementary data related to this article can be found at http://dx.doi.org/10.1016/j.jpowsour.2013.02.070.

References

[1] A.S. Arico, P. Bruce, B. Scrosati, J.-M. Tarascon, W. van Schalkwijk, Nat. Mater. 4 (2005) 366–377.
[2] M. Armand, J.M. Tarascon, Nature 451 (2008) 652–657.
[3] G.G. Amatucci, F. Badway, A.D. Pasquier, T. Zheng, J. Electrochem. Soc. 148 (2001) A930–A939.
[4] K.M. Colbow, J.R. Dahn, R.R. Haering, J. Power Sources 26 (1989) 397–402.
[5] E.M. Sorensen, S.J. Barry, H.-K. Jung, J.M. Rondinelli, J.T. Vaughey, K.R. Poeppelmeier, Chem. Mater. 18 (2005) 482–489.
[6] C.H. Chen, J.T. Vaughey, A.N. Jansen, D.W. Dees, A.J. Kahaian, T. Goacher, M.M. Thackeray, J. Electrochem. Soc. 148 (2001) A102–A104.
[7] K. Zaghib, M. Simoneau, M. Armand, M. Gauthier, J. Power Sources 81–82 (1999) 300–305.
[8] Y.-R. Jhan, C.-Y. Lin, J.-G. Duh, Mater. Lett. 65 (2011) 2502–2505.
[9] C.C. Li, Q.H. Li, L.B. Chen, T.H. Wang, ACS Appl. Mater. Interfaces 4 (2012) 1233–1238.
[10] A. Nugroho, W. Chang, S. Jin Kim, K. Yoon Chung, J. Kim, RSC Adv. 2 (2012) 10805–10808.
[11] Y.-Q. Wang, L. Gu, Y.-G. Guo, H. Li, X.-Q. He, S. Tsukimoto, Y. Ikuhara, L.-J. Wan, J. Am. Chem. Soc. 134 (2012) 7874–7879.
[12] Z. Wang, G. Xie, L. Gao, J. Nanomater. 2012 (2012) 7.
[13] H. Xiang, B. Tian, P. Lian, Z. Li, H. Wang, J. Alloys Compd 509 (2011) 7205–7209.
[14] L. Cheng, J. Yan, G.-N. Zhu, J.-Y. Luo, C.-X. Wang, Y.-Y. Xia, J. Mater. Chem. 20 (2010) 595–602.
[15] C. Jiang, M. Ichihara, I. Honma, H. Zhou, Electrochim. Acta 52 (2007) 6470–6475.
[16] J. Li, Z. Tang, Z. Zhang, Electrochem. Commun. 7 (2005) 894–899.
[17] S.C. Lee, S.M. Lee, J.W. Lee, J.B. Lee, S.M. Lee, S.S. Han, H.C. Lee, H.J. Kim, J. Phys. Chem. C 113 (2009) 18420–18423.
[18] Y. Li, G.L. Pan, J.W. Liu, X.P. Gao, J. Electrochem. Soc. 156 (2009) A495–A499.
[19] J. Kim, J. Cho, Electrochem. Solid-State Lett. 10 (2007) A81–A84.
[20] J. Chen, L. Yang, S. Fang, Y. Tang, Electrochim. Acta 55 (2010) 6596–6600.
[21] J. Liu, X. Li, J. Yang, D. Geng, Y. Li, D. Wang, R. Li, X. Sun, M. Cai, M.W. Verbrugge, Electrochim. Acta 63 (2012) 100–104.
[22] K. Amine, I. Belharouak, Z. Chen, T. Tran, H. Yumoto, N. Ota, S.-T. Myung, Y.-K. Sun, Adv. Mater. 22 (2010) 3052–3057.
[23] Y. Ren, A.R. Armstrong, F. Jiao, P.G. Bruce, J. Am. Chem. Soc. 132 (2009) 996–1004.
[24] J. Chen, L. Yang, S. Fang, S.-i. Hirano, K. Tachibana, J. Power Sources 200 (2012) 59–66.
[25] J. Haetge, P. Hartmann, K. Brezesinski, J. Janek, T. Brezesinski, Chem. Mater. 23 (2011) 4384–4393.
[26] K.-C. Hsiao, S.-C. Liao, J.-M. Chen, Electrochim. Acta 53 (2008) 7242–7247.
[27] C. Jiang, Y. Zhou, I. Honma, T. Kudo, H. Zhou, J. Power Sources 166 (2007) 514–518.
[28] E. Kang, Y.S. Jung, G.-H. Kim, J. Chun, U. Wiesner, A.C. Dillon, J.K. Kim, J. Lee, Adv. Funct. Mater. 21 (2011) 4349–4357.
[29] L. Shen, C. Yuan, H. Luo, X. Zhang, K. Xu, Y. Xia, J. Mater. Chem. 20 (2010) 6998–7004.
[30] Y. Tang, L. Yang, S. Fang, Z. Qiu, Electrochim. Acta 54 (2009) 6244–6249.
[31] Y. Tang, L. Yang, Z. Qiu, J. Huang, J. Mater. Chem. 19 (2009) 5980–5984.
[32] S.-W. Woo, K. Dokko, K. Kanamura, Electrochim. Acta 53 (2007) 79–82.
[33] S.-H. Yu, A. Pucci, T. Herntrich, M.-G. Willinger, S.-H. Baek, Y.-E. Sung, N. Pinna, J. Mater. Chem. 21 (2011) 806–810.
[34] L. Zhao, Y.-S. Hu, H. Li, Z. Wang, L. Chen, Adv. Mater. 23 (2011) 1385–1388.
[35] G.-N. Zhu, H.-J. Liu, J.-H. Zhuang, C.-X. Wang, Y.-G. Wang, Y.-Y. Xia, Energy Environ. Sci. 4 (2011) 4016–4022.
[36] L. Shen, C. Yuan, H. Luo, X. Zhang, L. Chen, H. Li, J. Mater. Chem. 21 (2011) 14414–14416.
[37] J. Kim, Y.-S. Park, B. Veriansyah, J.-D. Kim, Y.-W. Lee, Chem. Mater. 20 (2008) 6301–6303.
[38] B. Veriansyah, H. Park, J.-D. Kim, B.K. Min, Y.H. Shin, Y.-W. Lee, J. Kim, J. Supercrit. Fluids 50 (2009) 283–291.
[39] B. Veriansyah, J.-D. Kim, B.K. Min, Y.H. Shin, Y.-W. Lee, J. Kim, J. Supercrit. Fluids 52 (2010) 76–83.
[40] A. Nugroho, B. Veriansyah, S.K. Kim, B.G. Lee, J. Kim, Y.-W. Lee, Chem. Eng. J. 193–194 (2012) 146–153.
[41] M.Q. Snyder, W.J. DeSisto, C.P. Tripp, Appl. Surf. Sci. 253 (2007) 9336–9341.
[42] A. Nugroho, S.J. Kim, K.Y. Chung, B.-W. Cho, Y.-W. Lee, J. Kim, Electrochem. Commun. 13 (2011) 650–653.
[43] A. Nugroho, S.J. Kim, K.Y. Chung, J. Kim, Electrochim. Acta (2012) 623–632.
[44] Y. Harada, N. Takami, H. Inagaki, Y. Yoshida, US Patent 0244442 A1, 2012.